

Scheduled to appear in the Feb. 2005 AJ

Unresolved $H\alpha$ Enhancements at High Galactic Latitude in the WHAM Sky Survey Maps

R. J. Reynolds, V. Chaudhary, G. J. Madsen, & L. M. Haffner

Department of Astronomy, University of Wisconsin-Madison, Madison WI 53706

ABSTRACT

We have identified 85 regions of enhanced $H\alpha$ emission at $|b| > 10^\circ$ subtending approximately 1° or less on the Wisconsin $H\alpha$ Mapper (WHAM) sky survey. These high latitude “WHAM point sources” have $H\alpha$ fluxes of 10^{-11} to 10^{-9} erg $\text{cm}^{-2} \text{s}^{-1}$, radial velocities within about 70 km s^{-1} of the LSR, and line widths that range from less than 20 km s^{-1} to about 80 km s^{-1} (FWHM). Twenty nine of these enhancements are not identified with either cataloged nebulae or hot stars and appear to have kinematic properties that differ from those observed for planetary nebulae. Another 14 enhancements are near hot evolved low mass stars that had no previously reported detections of associated nebulosity. The remainder of the enhancements are cataloged planetary nebulae and small, high latitude H II regions surrounding massive O and early B stars.

Subject headings: catalogs; stars:subdwarfs; stars:white dwarfs; ISM:H II regions; ISM: planetary nebulae

1. Introduction

The Wisconsin $H\alpha$ Mapper (WHAM) has provided the first large-scale survey of the distribution and kinematics of ionized interstellar hydrogen, covering the sky north of declination -30° with an angular resolution of about 1° and a velocity resolution of 12 km s^{-1} within approximately $\pm 100 \text{ km s}^{-1}$ of the LSR (Haffner et al 2003). This survey shows interstellar $H\alpha$ emission filling the sky, with loops, filaments, and other large emission enhancements superposed on a more diffuse background. However, in addition to these large-scale features, the survey also reveals numerous small $H\alpha$ emission regions that have angular sizes comparable to or less than WHAM’s 1° diameter beam. In narrow ($\approx 20 \text{ km s}^{-1}$) velocity

interval maps, these WHAM point sources stand out as intensity enhancements in a single beam (or two adjacent beams) within a region of fainter diffuse emission.

Below we briefly describe our procedure for identifying and characterizing these enhancements, and we list the resulting flux, radial velocity, and line width of the $H\alpha$ emission, along with any previously cataloged nebulosity or hot star that may be associated with the region. The nature of most of these emission regions is unknown.

2. Identification of “WHAM Point Sources”

The enhancements were identified through a systematic search “by eye” through the entire data cube of the WHAM survey. This consisted of examining regions of the sky approximately 100 to 400 square degrees in size within narrow (20 to 30 km s^{-1}) radial velocity intervals centered between -90 km s^{-1} and $+90 \text{ km s}^{-1}$ (LSR). To minimize confusion with structure within bright, larger scale emission features near the Galactic midplane, we confined the search to Galactic latitudes $|b| > 10^\circ$. We also avoided the radial velocity interval -15 to $+15 \text{ km s}^{-1}$ in directions toward the Orion-Eridanus bubble, where relatively bright high latitude $H\alpha$ emission features make the identification of “point sources” unreliable. A less subjective identification program was also carried out, which calculated for each of the approximately 37,000 survey spectra the difference between the spectrum in a given direction and the average spectrum of that direction’s nearest neighbors. Directions with an enhancement were then selected based upon whether the difference spectrum exhibited an emission feature that was significantly greater than the scatter in the intensities of the nearest neighbors within the velocity range of the feature. This second method yielded a factor of ten more “point sources identifications”. However, a cursory examination revealed that the vast majority of these were false positives associated with small angular scale fluctuations within the diffuse $H\alpha$ background. We concluded that confidence in the identification of a true enhancement above the background required an examination “by eye” of a relatively large ($\sim 10^\circ \times 10^\circ$) region of the surrounding sky, not just the six nearest neighbors. This allowed us to select only those enhancements that stood out most clearly against the background and was thus the more conservative approach. The survey was examined by two of us (VC and RJR) independently, and the good agreement between the two results suggests that the enhancement identifications are robust, with $H\alpha$ surface brightnesses measured down to about 0.3 R ($1 \text{ R} = 10^6/4\pi \text{ photons cm}^{-2} \text{ s}^{-1} \text{ sr}^{-1}$), corresponding to an $H\alpha$ flux of about $1 \times 10^{-11} \text{ erg cm}^{-2} \text{ s}^{-1}$ for sources subtending 1° . While this $H\alpha$ flux limit is not particularly low for a planetary nebula search, the surface brightness limit, corresponding to an emission measure of about $1 \text{ cm}^{-6} \text{ pc}$, is well below that of most planetary nebula searches.

The sensitivity of WHAM is further enhanced over low spectral resolution imaging in cases where the enhancement is Doppler shifted with respect to the often higher surface brightness emission associated with the ubiquitous warm ionized component of the interstellar medium (see below).

The $H\alpha$ flux, radial velocity, and line width associated with each enhancement was measured by subtracting from the spectrum toward the enhancement the average spectrum toward the nearest neighbors, and then fitting the resultant $H\alpha$ emission line with a Gaussian profile. Examples are presented in Figures 1 through 4, which show for four relatively faint enhancements the velocity interval beam map of an area surrounding the enhancement, the spectra in the source direction and its nearest neighbors, and the difference spectrum with the best-fit Gaussian and residuals. The intensity enhancements in these examples range from 1.3 R (Fig. 1) down to 0.5 R (Figs. 2 & 3) and, depending upon the brightness of the diffuse $H\alpha$ background, produce moderate (Fig. 2) to small (Fig. 4) increases in the total $H\alpha$ intensity on the sky. The high spectral resolution of the WHAM survey has made possible the detection of sources (e.g., Fig. 4) that would be masked by the $H\alpha$ background and its variation in maps of total $H\alpha$ intensity. For these examples, there are no associations with previously reported nebulae (i.e., listed either in SIMBAD or in Cahn, Kaler, and Stanghellini 1992). In one of these examples (Fig. 2), the enhanced emission appears to be associated with a hot evolved low mass star (DA white dwarf), while for the other three no cataloged hot star is associated with the ionized region (see §3).

Seven of the enhancements occupy two adjacent pixels on the sky (e.g., Fig. 4), rather than being confined to a single WHAM beam. With one exception (WPS 6), we have assumed that these are situations in which the emission region is located near the edge of a beam, extending into the second beam. In these cases, we summed the two spectra, and the coordinates of the enhancement refer to the mean position of the two beams. For the two-pixel source WPS 6 at $l = 33^\circ 8$, $b = -22^\circ 1$ and $l = 34^\circ 1$, $b = -21^\circ 2$, the results in Table 1 are listed separately for each beam because there is a significant velocity shift associated with the enhancement between the two directions (Fig. 5), suggesting two independent sources (see §4)

3. Results

Table 1 lists in order of increasing Galactic longitude the identified “WHAM point sources” (WPS) and the results of the Gaussian fits to the difference spectra. Following the WPS number are the Galactic coordinates of the center of the WHAM survey beam (for single pixel sources) plus the $H\alpha$ flux, radial velocity, and line width (FWHM) for each of

the enhancements. The enhancements WPS 6-1 and WPS 6-2, while in adjacent pixels, are treated as two separate H II regions (see §4), while WPS 65 is a planetary nebula exhibiting two resolved H α velocity components (Recillas-Cruz & Pişmiş 1981). The H α flux is based on a calibration using those enhancements identified as planetary nebulae (see Table 2) and for which H β fluxes and reddening measurements have been published (Cahn et al 1992). The errors in the fitted parameters are dominated by the uncertainty in the baseline of the difference spectrum and/or by the scatter in the data points of the spectrum (e.g., see Figs. 1 - 4). Errors due to baseline uncertainty were estimated by fitting each difference spectrum multiple times with different fixed baselines. Errors due to scatter in the spectral data points were determined by the standard deviation calculation carried out by the least-squares Gaussian fitting program. The listed errors for each parameter represent the largest uncertainties determined by these methods.

Table 2 lists for each enhancement the celestial coordinates (2000.0) of the center of the beam (or the mean position for two-pixel sources), the name of any cataloged nebulae near that direction, the name of a candidate ionizing star (if there is no cataloged nebula), the spectral type of the star, and the off-set of the nebula or star from the center of the beam. The resources for the ionizing star and nebula searches were SIMBAD and the planetary nebula catalog by Cahn et al (1992). When no cataloged nebula was listed within 40' of the beam center, a search for an ionizing star was carried out on SIMBAD to a radius of 60'.

4. Discussion

Of the 85 H α enhancements identified, more than half (44) are not associated with any previously cataloged nebula, and of these, fifteen are associated with hot evolved low mass stars, including one DO and seven DA white dwarfs, three SdO, and two SdB stars (Table 2). This is a potential source of new information about the natures of these evolved stars and their evolution (Tweedy & Kwitter 1994). For example, because of WHAM's large beam, some of these enhancements could be associated with large planetary nebulae in very late stages of their evolution having surface brightnesses that are too faint to have been detected on earlier searches. The identification of the nebulosity with the star is most certain for those stars within the WHAM beam (i.e., angular offsets < 30'). However, because large, highly evolved planetary nebulae can be offset significantly from their ionizing stars (Tweedy & Napiwotzki 1994; Borkowski, Sarazin, & Soker 1990; Reynolds 1985), we have considered stars located up to 1° from the directions listed in the Tables. We confirm the earlier detection of ionized gas associated with the DO white dwarf PG 0108+101 (Reynolds 1987) and provide improved kinematic information about that H II region.

Twenty nine emission regions could not be associated with either a cataloged nebula or hot star. This could be the result of incompleteness in the SIMBAD listings, or it could indicate another kind of nebulosity. These enhancements have a mean line width near 27 km s^{-1} , significantly smaller than that (38 km s^{-1}) of the cataloged planetary nebulae. This is illustrated in Figure 6, which compares histograms of line widths for three categories of WHAM point sources: enhancements not associated with any cataloged nebula or evolved hot star, enhancements near a hot low mass star, enhancements associated cataloged planetary nebulae (the six regions associated with massive O and B stars are excluded from these histograms). We found no associations with supernova remnants or Herbig-Hero objects, although WPS 11 and WPS 21 are within $37'$ and $48'$ of the two high Galactic latitude molecular clouds, MBM 50 and MBM 46, respectively, which could harbor star formation activity. However, the narrow line widths appear to rule out such shock excited sources, as well as any association with emission line stars, which exhibit line widths in excess of $60 - 100 \text{ km s}^{-1}$ (e.g., Hartigan et al 1987; Hamann & Persson 1992a,b). It is tempting to speculate that these emission regions are associated with the most evolved planetary nebulae, those whose expansion has been halted by interactions with the ambient interstellar medium (Tweedy & Napiwotzki 1994; Reynolds 1985), or those whose gas has thinned to such an extent that it is the ambient interstellar medium itself that has become the primary H II region (Borkowski, Sarazin, & Soker 1990). Followup, high angular resolution imaging of these regions could help to discriminate between the possibilities (Soker, Borkowski, & Sarazin 1991). Figures 7 and 8 show corresponding histograms for radial velocity and $\text{H}\alpha$ flux. No clear differences between the three categories of enhancements are apparent in these distributions. In Figures, 6, 7, and 8, the V_{LSR} and FWHM used for WPS 65 are the flux weighted average radial velocity (i.e., $+19 \text{ km s}^{-1}$) and the separation (i.e., 37 km s^{-1}) of the two velocity components, respectively.

Six of the enhancements appear to be small H II regions associated with massive late O and early B type stars. The region near the B1 V star HD 191639 (WPS 6) was detected in two pixels and exhibits a significant (21 km s^{-1}) radial velocity difference between the two directions (Fig. 5). This suggests either peculiar, small-scale kinematic variations within the region or the existence of two independent H II regions closely spaced on the sky. In this latter case, because the B star has a radial velocity of $-7 \pm 5 \text{ km s}^{-1}$ (Wilson 1953), the emission region produced by the B star would be more likely associated with the enhancement (WPS 6-1) at $-10 \pm 2 \text{ km s}^{-1}$ toward $l = 33^\circ 8$, $b = -22^\circ 1$, while the emission (WPS 6-2) at $+11 \text{ km s}^{-1}$ toward $l = 34^\circ 1$, $b = -21^\circ 2$ would have no identified source of ionization (for Figs. 6, 7, & 8, we have assumed this latter case). Enhancements WPS 23, 60, 68, and 72 have late B stars (B6 V, B9, B9, and B8/B9II, respectively) located $34'$ to $43'$ away. Because the Lyman continuum fluxes from such late type B stars are predicted to be orders of magnitude

weaker than the fluxes of the early B stars discussed above, we have concluded that these associations are coincidences.

5. Summary and Conclusions

From the WHAM sky survey we have identified and measured the fluxes, radial velocities, and line widths for 85 regions of H α enhancement at Galactic latitudes $|b| > 10^\circ$ that appear to subtend approximately one degree or less on the sky. Most of these ionized regions have not been previously reported as emission nebulae, and their nature is unknown. A next step is to carry out additional observations to determine the morphology of these emission regions and their sources of ionization. This will include spectra of [O III] $\lambda 5007$, [N II] $\lambda 6584$, and [S II] $\lambda 6716$ to explore the ionization and excitation state of the gas, as well as observations using WHAM’s “imaging mode” to obtain deep, very narrow band (30 km s^{-1}) images of these enhancements at an angular resolution at about $3'$ within a 1° field of view (Reynolds et al 1998).

We thank an anonymous referee for helpful comments. This work was funded by the National Science Foundation through grants AST96-19424 and AS02-04973. The WHAM survey was funded by the National Science Foundation through grants AST 91-22701 and AST 96-19424 with assistance from the University of Wisconsin’s Graduate School, Department of Astronomy, and Department of Physics. This research has made use of the SIMBAD database, operated at CDS, Strasbourg, France.

REFERENCES

- Borkowski, K. J. Sarazin, C. L., & Soker, N. 1990 ApJ 360, 173
- Hamann, F. & Persson, S. E. 1992a ApJS 82, 247
- Hamann, F. & Persson, S. E. 1992b ApJS 82, 285
- Cahn, J. H., Kaler, J. B., & Stanghellini, L. 1992 A&AS 94, 399
- Haffner, L. M., Reynolds, R. J., Tufte, S. L., Madsen, G. J., Jaehnig, K. P., & Percival, J. W. 2003 ApJS 149, 405
- Hartigan, P., Raymond, J., & Hartmann, L. 1987 ApJ 316, 323

- Recillas-Cruz, E. & Pişmiş, P. 1981 A&A 97, 398
- Reynolds R. J. 1985, ApJ 288, 622
- Reynolds, R. J. 1987, ApJ 315, 234
- Reynolds, R. J., Tufte, S. L., Haffner, L. M., Jaehnig, K., & Percival, J. W. 1998, Publ. Astron. Soc. Aust. 15, 14
- Soker, N., Borkowski, K. J., & Sarazin, C. L. 1991, AJ 102, 1381
- Tweedy, R. E. & Kwitter, K. B. 1994, ApJ 433, L93
- Tweedy, R. E., & Napiwotzki, R. 1994, AJ 108, 188
- Wilson, R. E. 1953, General Catalogue of Stellar Radial Velocities, Carnegie Institution of Washington D. C. Publ. 601

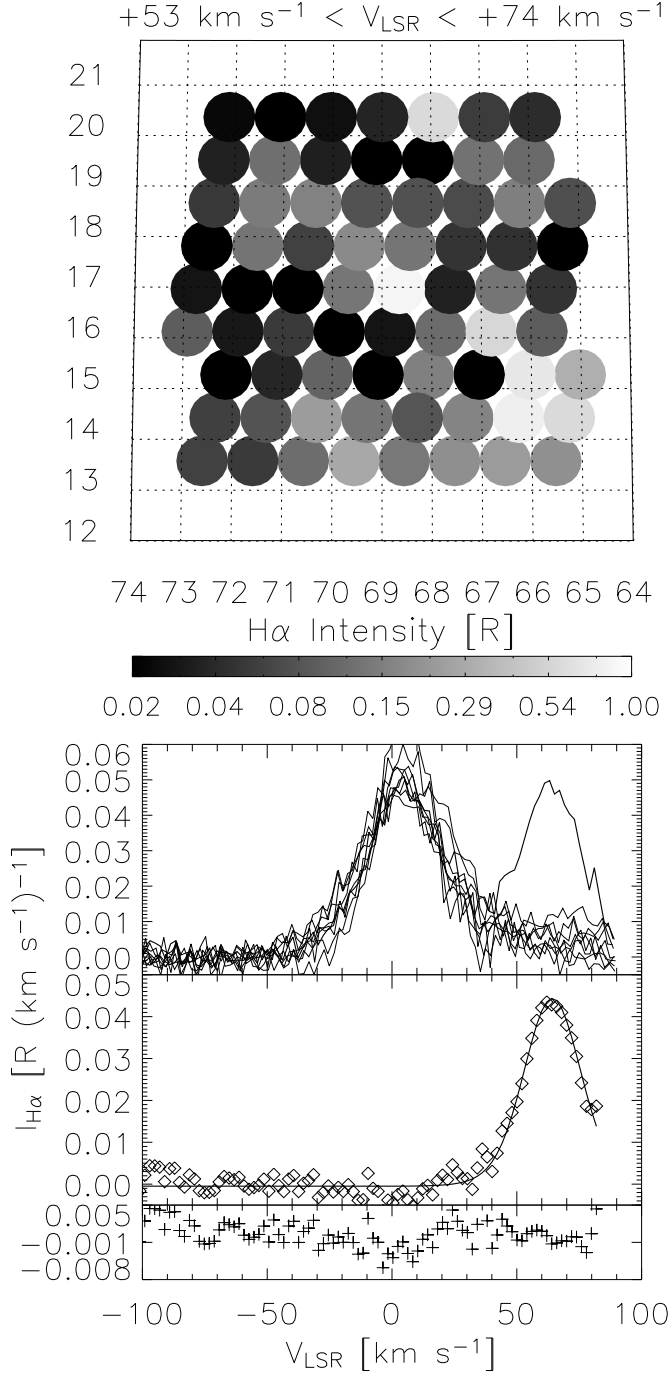


Fig. 1.— Top: a radial velocity interval map of a small portion of the WHAM H α sky survey showing the intensity enhancement toward WHAM Point Source (WPS) 20, at $l = 68^\circ 7$, $b = +17^\circ 0$. The circles represent the WHAM beams and the grey scale denotes the H α intensity within each beam (in rayleighs). The coordinates are degrees of Galactic longitude (abscissa) and latitude (ordinate). Bottom: H α spectra (solid lines) toward WPS 20 and its nearest neighbors; the difference spectrum (diamonds) with its single-Gaussian best-fit and residuals (crosses); see §2. in text. The H α line centered near 0 km s^{-1} in all of the spectra is emission associated with the widespread warm ionized component of the interstellar medium (e.g., Haffner et al 2003).

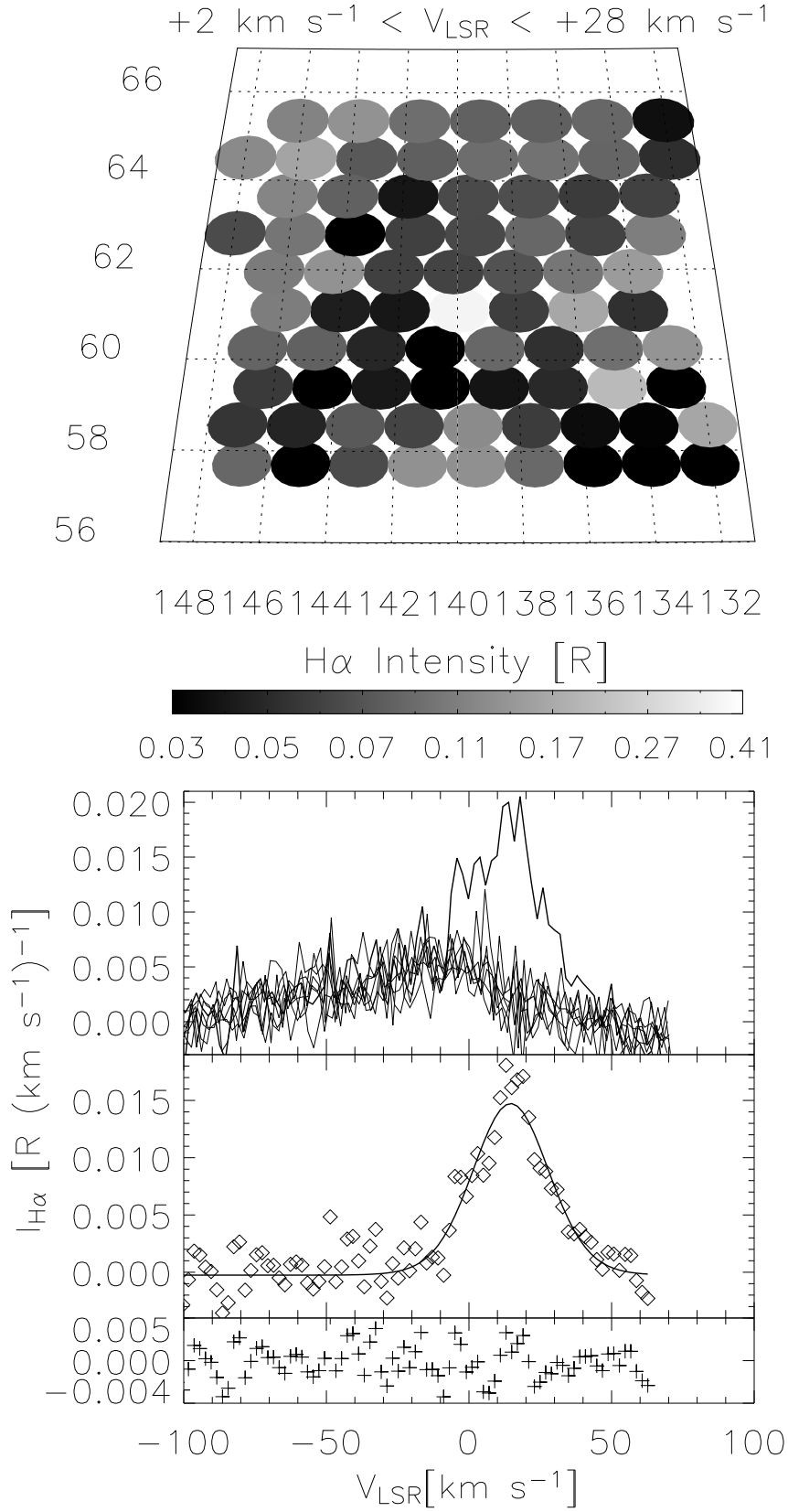


Fig. 2.— Same as Fig 1. except for WPS 43.

– 10 –

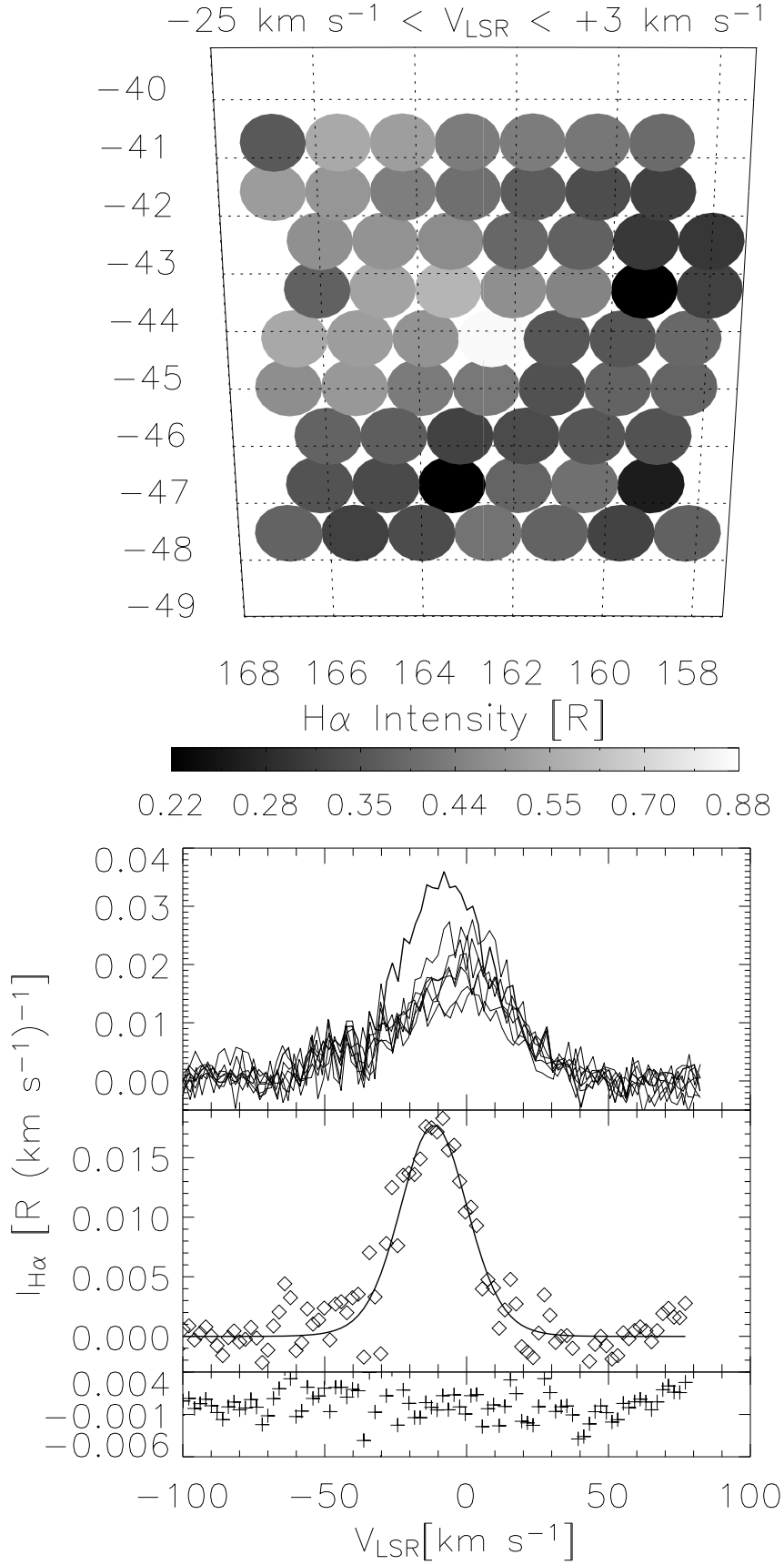


Fig. 3.— Same as Fig 1. except for WPS 53.

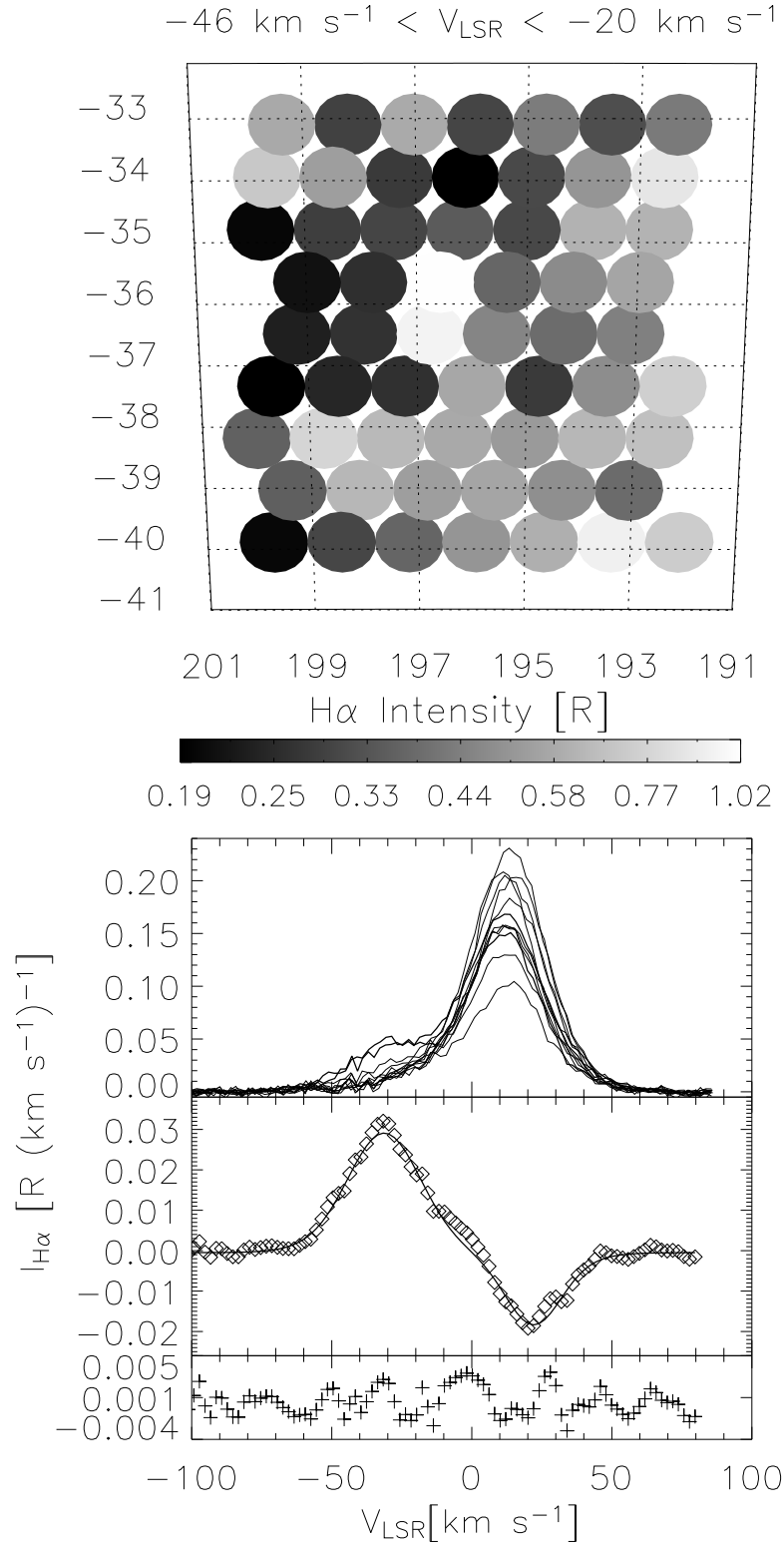


Fig. 4.— Same as Fig 1. except for WPS 63. Note that this is a two-pixel enhancement. The parameters for this source listed in Table 1 refer to the positive-area Gaussian centered at about -30 km s^{-1} in the difference spectrum.

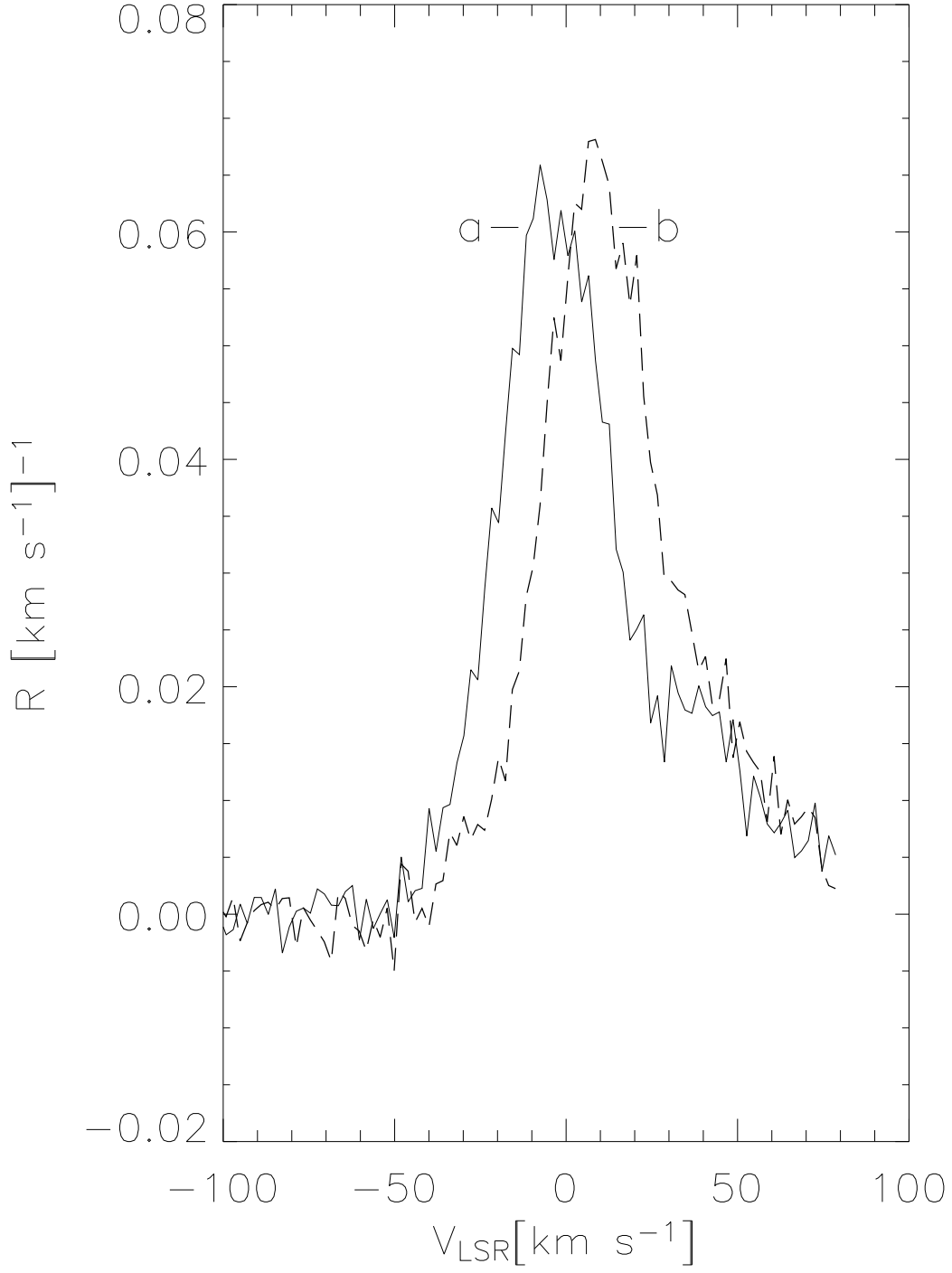


Fig. 5.— $H\alpha$ difference spectra toward WPS 6-1 and WPS 6-2. a: $l = 33^\circ 8$, $b = 22^\circ 1$; b: $l = 34^\circ 1$, $b = -21^\circ 2$.

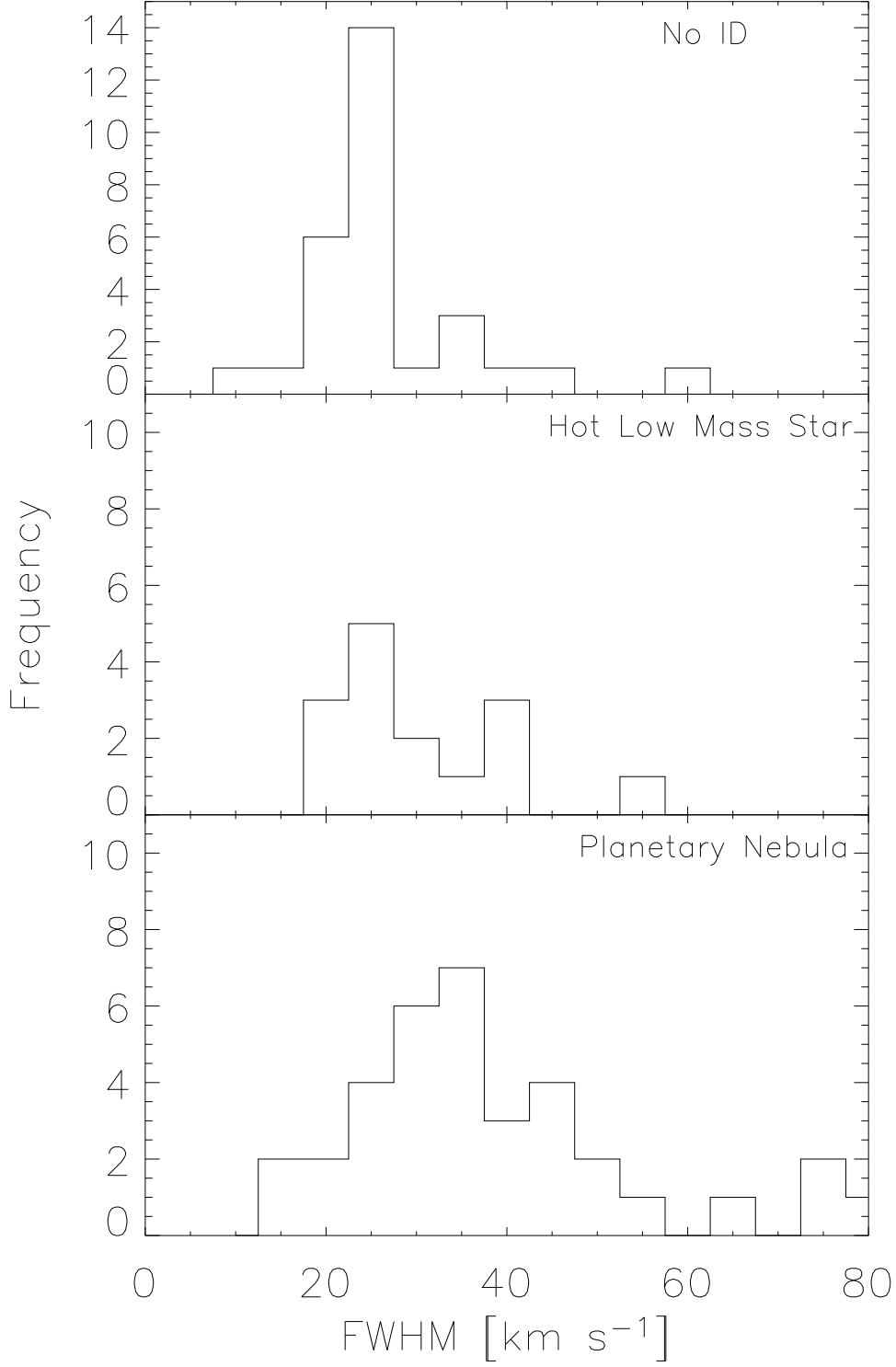


Fig. 6.— Histograms of the number of enhancements versus FWHM of the H α emission line. Top: enhancements not associated with any previously catalogued nebula nor any identified ionizing source. Middle: enhancements not associated with any previously catalogued nebula but with a hot evolved low mass star located within one degree of the center of the WHAM beam. Bottom: enhancements associated with catalogued planetary nebulae.

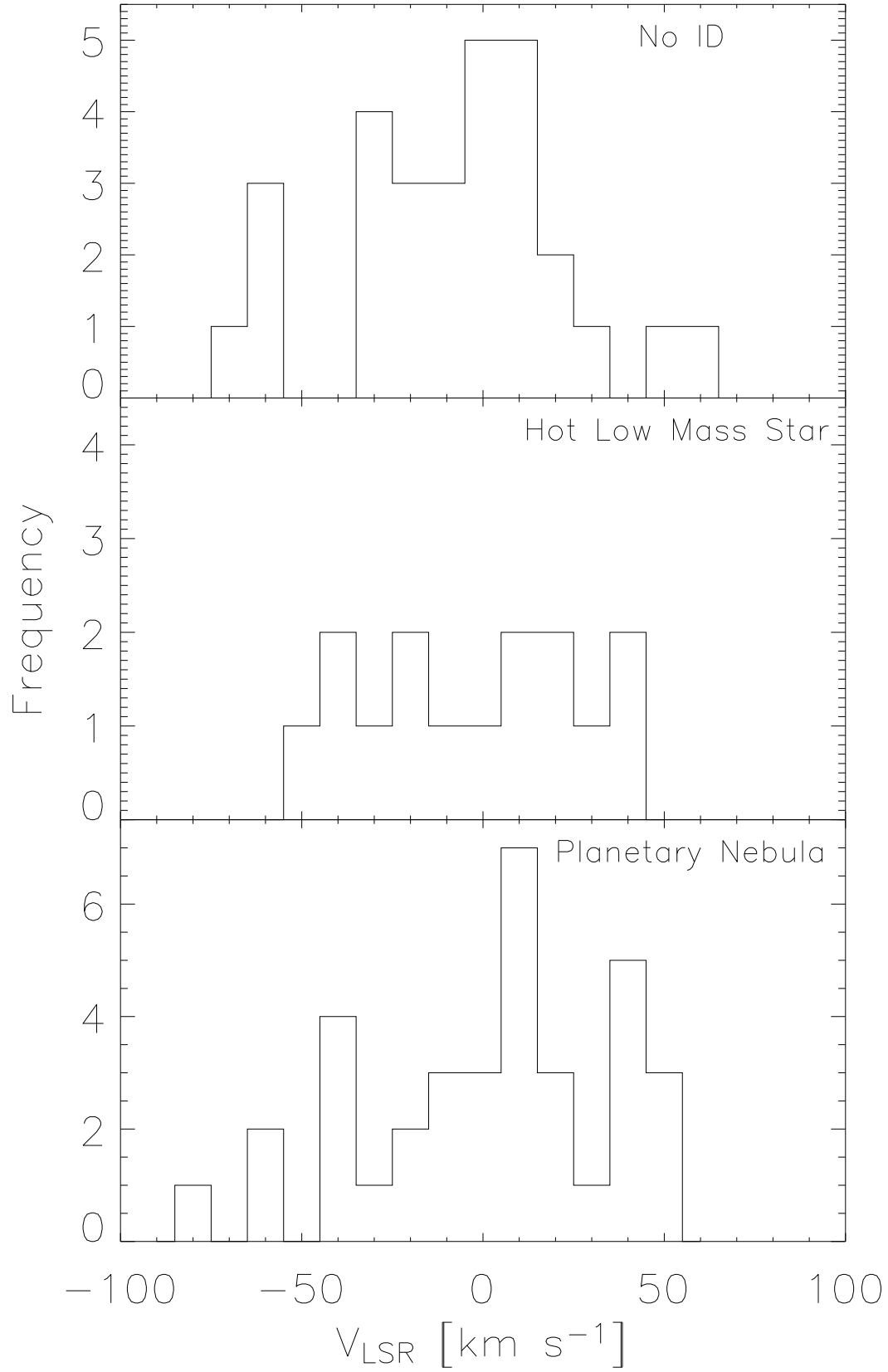


Fig. 7.— Same as Fig. 6, except histograms of the radial velocity of the H α emission.

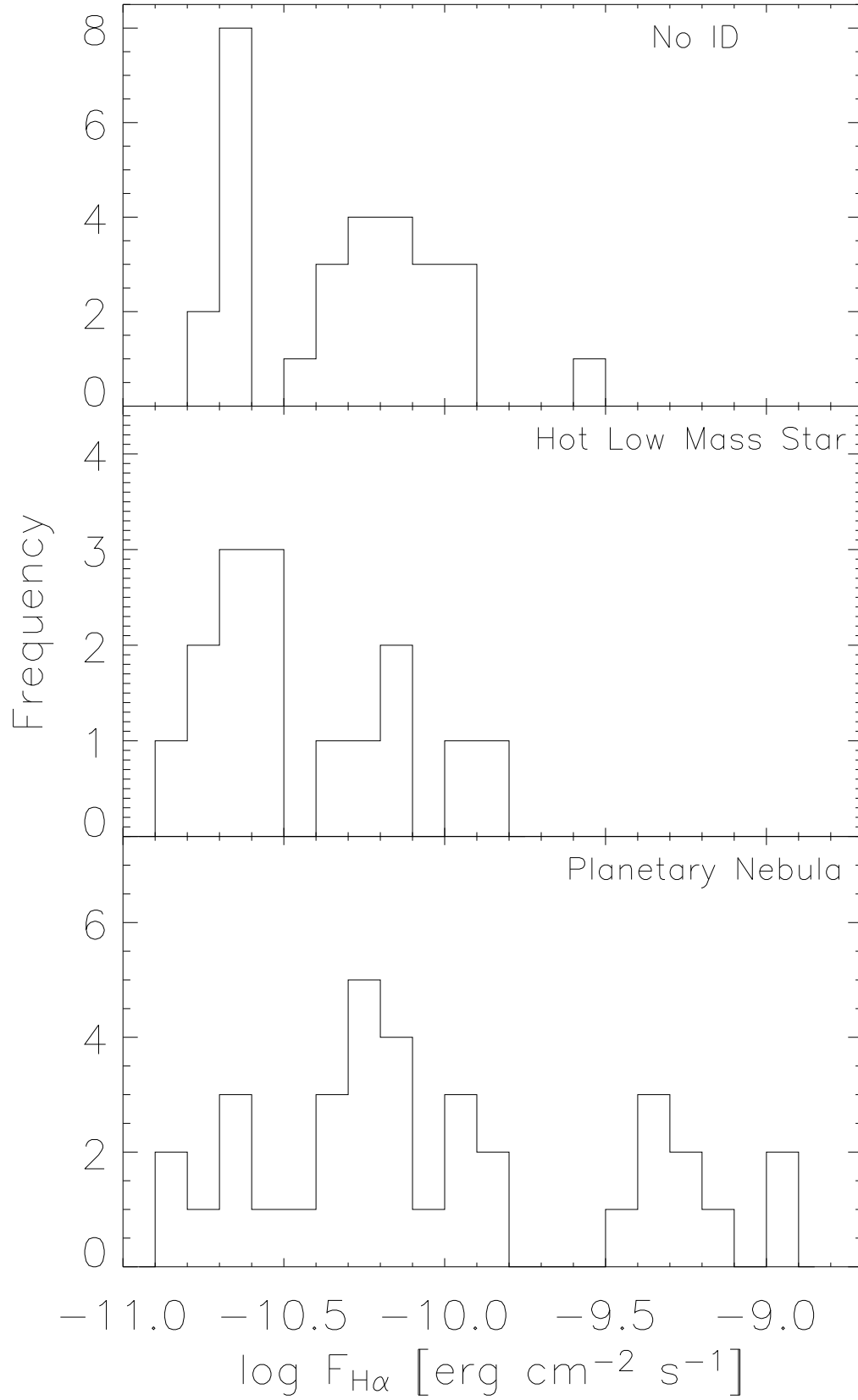


Fig. 8.— Same as Fig. 6, except histograms of the flux of the H α emission.

Table 1. Results for High Latitude Wham Point Sources

WPS	l (deg)	b (deg)	$F_{H\alpha}$ (10^{-11}) ^a	V_{LSR} (km s ⁻¹)	FWHM (km s ⁻¹)
1	23.14	-17.83	13.8±1.7	+38±1	39±3
2	23.76	-14.43	8.8±0.8	+47±1	18±2
3	25.87	+40.74	7.9±0.8	+41±1	29±3
4	26.20	+46.68	2.9±1.3	-4±6	56±15
5	26.23	-17.83	8.8±1.7	+14±2	43±4
6-1 ^b	33.84	-22.07	5.0±0.8	-10±2	24±4
6-2 ^b	34.13	-21.22	4.2±1.3	+11±2	25±5
7	35.05	+11.88	56.8±1.3	+11±1	35±12
8	36.35	-56.86	111.2±2.5	-24±1	40±5
9	37.49	-34.80	51.8±4.2	-40±2	45±1
10	38.06	+11.88	5.4±0.8	+39±2	24±4
11 ^c	39.84	-35.23	10.8±1.7	+26±3	25±5
12 ^c	43.01	+37.77	40.1±1.7	-20±1	23±2
13	44.77	-46.68	2.1±0.4	-28±4	34±6
14	45.76	+24.61	2.9±0.8	0±2	22±6
15	54.08	-11.88	10.9±2.1	+48±3	51±4
16 ^c	55.00	-14.86	7.5±1.7	+13±2	21±3
17	57.03	+43.28	8.4±4.2	-69±4	22±12
18	58.40	-11.03	7.1±2.1	-40±7	39±15
19	65.56	+22.07	2.9±0.8	-37±3	27±10
20	68.65	+16.97	5.4±0.8	+64±1	21±3
21	69.31	-18.67	6.3±0.8	+52±2	27±4
22	69.42	-30.55	3.3±0.8	+30±4	36±14
23	71.38	+18.67	9.2±0.8	+17±1	27±4
24	72.75	-16.97	5.0±0.8	+43±5	23±7
25	74.85	-36.49	4.6±0.8	+10±3	32±5
26	83.73	+72.99	2.1±0.8	-24±5	37±13
27	83.88	+12.73	47.2±2.9	+13±1	34±1
28	91.99	+19.52	3.3±0.8	+6±3	27±6
29	96.39	+29.70	78.6±2.9	-55±1	37±1
30	106.52	-17.82	36.8±1.3	-10±1	49±2
31	109.82	+21.22	7.5±0.4	-22±1	20±2

Table 1—Continued

WPS	l (deg)	b (deg)	$F_{H\alpha}$ (10^{-11}) ^a	V_{LSR} (km s ⁻¹)	FWHM (km s ⁻¹)
32	110.16	-11.88	2.5±0.8	+50±4	31±9
33	118.60	+39.04	2.5±0.8	+15±3	24±8
34	118.75	-74.69	5.9±2.1	34±10	73±20
35	120.00	+18.67	7.1±0.8	+4±1	25±1
36	123.41	+34.80	5.4±0.8	-35±2	34±4
37	126.19	-46.68	1.7±0.4	+6±1	20±3
38	130.75	-52.62	2.1±0.8	-14±3	21±8
39	133.11	+12.73	4.6±0.8	-33±2	27±5
40	133.22	-40.74	1.3±0.4	-36±4	22±13
41	137.39	-24.61	5.4±1.3	-63±2	26±3
42	139.24	+45.83	2.1±0.8	-57±7	47±14
43	139.94	+61.11	2.1±0.8	+15±4	26±11
44	142.11	-28.86	5.4±1.3	-26±4	58±8
45	142.23	+15.28	1.3±0.4	-79±2	13±4
46 ^c	143.86	+38.62	5.0±0.8	-52±2	31±5
47	146.70	-23.76	2.9±0.8	+30±4	39±7
48	149.29	+56.86	5.9±1.7	+15±5	79±11
49	159.02	+17.82	5.9±0.8	+7±2	37±5
50	159.02	+37.34	2.1±0.8	-9±5	28±13
51	160.62	-23.76	11.3±3.3	+9±1	23±2
52	161.20	-26.31	7.5±1.3	+8±1	22±3
53	162.48	-44.13	2.1±0.4	-11±3	28±7
54	162.55	+47.53	1.7±0.8	-19±5	38±14
55	163.94	-16.97	13.8±1.3	-6±1	17±1
56	164.68	+31.40	2.1±8.4	-60±5	44±15
57	165.59	-15.28	4.2±0.8	+42±4	42±10
58	166.28	+10.18	10.0±0.8	-39±1	31±2
59	174.73	+15.28	10.0±1.3	-33±1	27±3
60	181.26	+11.88	7.1±1.3	-2±1	24±3
61	191.42	+40.74	1.7±0.4	+5±7	32±19
62	193.44	-24.61	1.5±2.9	-11±1	14±2
63 ^c	196.66	-36.07	9.2±1.7	-33±1	26±2

Table 1—Continued

WPS	l (deg)	b (deg)	$F_{H\alpha}$ (10^{-11}) ^a	V_{LSR} (km s ⁻¹)	FWHM (km s ⁻¹)
64	199.45	-22.92	4.2±0.4	-63±2	23±4
65 ^d	204.90	+14.43	7.5±0.8	+2±3	22±10
65 ^d	204.90	+14.43	6.3±1.3	+39±2	28±8
66	211.31	+11.88	6.7±0.7	+3±1	20±2
67	215.00	-24.61	100.7±2.1	+44±1	28±2
68	216.18	-67.89	2.1±0.8	-12±5	34±13
69	217.07	+28.86	11.7±2.5	-3±1	20±2
70	218.64	+31.40	4.6±1.3	+22±3	54±7
71	220.09	-54.31	11.3±1.3	+49±3	73±5
72	223.71	-20.37	29.3±1.7	-7±1	17±1
73	235.12	+47.53	1.7±0.4	+16±5	35±12
74	235.17	+29.70	5.4±0.8	+6±2	25±5
75	243.09	+36.49	2.5±0.4	0±3	24±7
76	260.73	+32.25	48.1±2.5	+1±1	43±1
77	264.29	+50.92	1.7±0.4	-3±5	26±10
78	293.97	+43.28	7.5±1.3	+12±7	67±15
79	303.20	+39.89	15.1±0.4	-12±1	28±2
80	312.12	+67.05	2.5±0.8	-23±2	12±7
81	315.00	+36.49	2.5±0.8	+39±5	40±14
82 ^c	337.44	+47.53	6.7±1.7	-17±2	26±5
83	347.06	+20.37	219±29	+1±1	21±1
84	351.45	+16.97	493±50	0±1	20±1

^aerg cm⁻² s⁻¹.

^bTwo-pixel point source where the radial velocity is different in each beam; see text.

^cDenotes two-pixel point source.

^dOne-pixel point source with 2 emission peaks.

Table 2. Wham Point Source Identifications

WPS	RA	Dec	Nebula	Star	Spectral Type	Beam Offset (Arc Minutes)
1	19 39.3	-16 29	...	LSE 22	O+	56
2	19 27.4	-14 32	...	V4372 Sgr	B2 IV	38
3	16 12.8	+12 24	PN IC 4593	25
4	15 51.0	+15 05	...	PG 1548+149	DA	18
5	19 54.9	-13 48	PN NGC 6818	22
6	20 11.0	-08 48	...	HD 191639	B1 V	4
7	18 12.7	+07 15	PN NGC 6572	25
8	22 28.7	-20 40	PN NGC 7293	17
9	21 04.6	-11 40	PN NGC 7009	19
10	18 18.0	+09 53	PN PHL 932	16
11	21 09.6	-10 07
12	16 44.4	+23 44	PN NGC 6210	5
13	21 58.1	-11 55
14	17 41.7	+21 41	PN G045.6+24.3 (K1-14)	19
15	20 14.1	+12 44	PN NGC 6891	16
16	20 26.4	+11 54
17	16 29.3	+35 15
18	20 11.8	+13 27	PN IC4997	5
19	18 20.3	+38 02	...	FBS 1815+381	DA	35
20	18 49.9	+39 03
21	21 12.9	+20 44
22	21 50.4	+12 57	PN LBN 069.67-30.36	16
23	18 46.4	+42 05
24	21 16.5	+24 20	PN PK072-17 (A74)	7

Table 2—Continued

WPS	RA	Dec	Nebula	Star	Spectral Type	Beam Offset (Arc Minutes)
25	22 20.7	+11 56	...	31 Peg	B2 IV-Ve	21
26	13 47.0	+39 38
27	19 46.1	+50 46	PN NGC 6826	19
28	19 24.9	+60 40
29	18 01.1	+66 34	PN NGC 6543	15
30	23 26.1	+42 19	PN NGC 7662	13
31	20 25.3	+76 40	...	KUV20417+7604	sd:O	60
32	23 34.3	+49 04	PN PP105 (K1-20)	51
33	13 54.6	+77 33
34	00 46.9	-11 51	PN NGC 246	2
35	23 38.2	+81 07	PN LBN 120.29+18.39	26
36	12 39.7	+82 19	PN IC 3568	20
37	01 00.7	+16 08	PN PHL 932	26
38	01 10.7	+09 58	...	PG 0108+101	DO	25
39	03 13.4	+72 44
40	01 24.9	+21 28	...	PG 0122+214	Sd?	12
41	01 57.0	+36 25
42	10 49.9	+67 16
43	11 55.6	+54 08	...	EGGR 435	DA	37
44	02 09.9	+31 04
45	04 53.3	+68 30	PN IRAS 04488+6903	28
46	09 25.8	+69 05	...	PG 0931+691	sd:O	57
47	02 37.3	+34 11	...	KUV 02335+3343	sdB	18 ^a
48	11 11.7	+54 52	PN NGC 3587	29

Table 2—Continued

WPS	RA	Dec	Nebula	Star	Spectral Type	Beam Offset (Arc Minutes)
49	06 19.6	+55 31	PN G158.9+17.8 (PW1)	6
50	08 42.6	+58 02	PN G158.8+37.1 (A28)	14
51	03 27.8	+27 27
52	03 22.7	+25 06
53	02 42.1	+10 05
54	09 48.4	+53 04
55	03 58.7	+30 37	...	X Per	O9.5pe	50
56	07 59.3	+53 33	PN G164.8+31.1	15
57	03 59.6	+32 44	PN NGC 1514	4
58	05 55.2	+45 51	PN IC 2149	19
59	06 40.1	+40 37	...	WD 0632+40	DA	45
60	06 37.4	+33 27
61	09 02.6	+33 01	...	CBS 90	DA	35
62	04 48.6	+04 36	PN HS 0444+453	35
63	04 16.9	-03 34
64	05 05.9	+00 47
65	07 29.3	+13 32	PN G205.1+14.2 (YM29)	18
66	07 31.0	+06 48
67	05 25.9	-12 39	PN IC 418	23
68	02 30.4	-26 12
69	08 42.2	+09 26
70	08 53.9	+09 19	PN PK 219+31 (A31)	25
71	03 31.5	-25 47	PN NGC 1360	25
72	05 55.6	-18 21

Table 2—Continued

WPS	RA	Dec	Nebula	Star	Spectral Type	Beam Offset (Arc Minutes)
73	10 15.5	+06 17	...	WD 1010+064	DA	31
74	09 16.7	-03 49	...	PG 0914+037	sd:O	10
75	09 54.6	-05 04
76	10 24.6	-18 19	PN NGC 3242	20
77	11 18.4	-04 50
78	12 23.5	-19 23	PN NGC 4361	22
79	12 52.3	-22 59	PN G303.6+40.0 (A35)	18
80	13 05.8	+04 26
81	13 34.3	-25 22	...	EC 13331-2540	sd:B	40
82	14 22.6	-09 08	...	G 124-26	DA	17
83	15 57.9	-26 07	...	Pi Sco	B1 V	13
84	16 21.7	-25 31	...	Sig Sco	B1 III	8

^aWD 0230+343 (DA) is within 52 arc minutes of beam center.